bioRxiv preprint doi: https://doi.org/10.1101/2024.09.21.614276; this version posted September 23, 2024. The copyright holder for this preprint (which was not certified by peer review) is the author/funder, who has granted bioRxiv a license to display the preprint in perpetuity. It is made available under a CC-BY 4.0 International license.

Neuroinvasive and neurovirulent potential of SARS-CoV-2 in the acute and post-acute phase of intranasally inoculated ferrets

Authors: Feline F. W. Benavides[1], Edwin J. B. Veldhuis Kroeze[1], Lonneke Leijten[1], Katharina S. Schmitz[1], Peter van Run[1], Thijs Kuiken[1], Rory D. de Vries[1], Lisa Bauer[1*], Debby van Riel[1*#]

Affiliations: [1]Department of Viroscience, Erasmus MC, Rotterdam, the Netherlands

*These authors contributed equally

[#]corresponding author: d.vanriel@erasmusmc.nl

Keywords: SARS-CoV-2, ferret, central nervous system, neuroinvasion, neurovirulence, microglial activation, astrocytic activation

bioRxiv preprint doi: https://doi.org/10.1101/2024.09.21.614276; this version posted September 23, 2024. The copyright holder for this preprint (which was not certified by peer review) is the author/funder, who has granted bioRxiv a license to display the preprint in perpetuity. It is made available under a CC-BY 4.0 International license.

Abstract

Severe acute respiratory syndrome corona virus 2 (SARS-CoV-2) can cause systemic disease, including neurological complications, even after mild respiratory disease. Previous studies have shown that SARS-CoV-2 infection can induce neurovirulence through microglial activation in the brains of patients and experimentally inoculated animals, which are models representative for moderate to severe respiratory disease. Here, we aimed to investigate the neuroinvasive and neurovirulent potential of SARS-CoV-2 in intranasally inoculated ferrets, a model for subclinical to mild respiratory disease. The presence of viral RNA, histological lesions, virus-infected cells, and the number and surface area of microglia and astrocytes were investigated. Viral RNA was detected in various respiratory tissue samples by qPCR at 7 days post inoculation (dpi). Virus antigen was detected in the nasal turbinates of ferrets sacrificed at 7 dpi and was associated with inflammation. Viral RNA was detected in the brains of ferrets sacrificed 7 dpi, but *in situ* hybridization nor immunohistochemistry did not verify evidence of infection. Histopathological analysis of the brains showed no evidence for an influx of inflammatory cells. Despite this, we observed an increased number of Alzheimer type II astrocytes in the hindbrains of SARS-CoV-2 inoculated ferrets. Additionally, we detected an increased microglial activation in the olfactory bulb and hippocampus, and a decrease in the astrocytic activation status in the white matter and hippocampus of SARS-CoV-2 inoculated ferrets. In conclusion, although showed that SARS-CoV-2 has limited neuroinvasive potential in this model for subclinical to mild respiratory disease, there is evidence for neurovirulent potential. This study highlights the value of this ferret model to study the neuropathogenecity of SARS-CoV-2 and reveals that a mild SARS-CoV-2 infection can affect both microglia and astrocytes in different parts of the brain.

bioRxiv preprint doi: https://doi.org/10.1101/2024.09.21.614276; this version posted September 23, 2024. The copyright holder for this preprint (which was not certified by peer review) is the author/funder, who has granted bioRxiv a license to display the preprint in perpetuity. It is made available under a CC-BY 4.0 International license.

Introduction

Severe acute respiratory syndrome coronavirus 2 (SARS-CoV-2) infection causes respiratory disease. Additionally, a broad variety of neurological symptoms has been reported occasionally the acute and post-acute phases. These neurological complications can occur after severe, mild or even subclinical respiratory disease and comprise a variety of symptoms. In the acute phase, symptoms including brain fog, headache and memory loss have been observed and several of these symptoms can also persist in the post-acute phase and are part of long-COVID (1,2). Yet, the pathogenesis of neurological disease resulting from SARS-CoV-2 infection is not fully understood.

SARS-CoV-2 has the ability for neuroinvasion, meaning that the virus can enter the peripheral or central nervous system (PNS, CNS) (3). Several studies have shown that SARS-CoV-2 can enter the CNS through axonal transport via several cranial nerves (the olfactory and trigeminal nerves, among others) or via the hematogenous route (3). One important route is via the olfactory mucosa (located in the nasal cavity) where replication of SARS-CoV-2 can result in virus spread through the cribriform plate into the olfactory bulb of the brain. In the olfactory mucosa of coronavirus disease 2019 (COVID-19) patients, SARS-CoV-2 replicates predominantly in sustentacular cells and rarely in olfactory receptor neurons based on the expression of viral antigen or viral RNA (4,5). In tissues obtained from human autopsies, viral RNA or virus antigen was detected in the olfactory bulb (5–8); however, other studies failed to confirm this (8,9). Virus antigen and viral RNA have been detected in neurons, astrocytes and oligodendrocytes in other areas of the human CNS, like the frontal lobe, hypothalamus, basal ganglia, cerebellum and spinal cord (9–13). In experimentally inoculation animals, virus antigen and viral RNA were detected in the olfactory bulb of cynomolgus macaques, ferrets, mice and hamsters (14–18), suggesting neuroinvasion via the olfactory nerve. *In vitro*, SARS-CoV-2 infects neurons in human brain organoids, human pluripotent stem cell (hPSC)-derived dopaminergic neurons and hPSC-derived

bioRxiv preprint doi: https://doi.org/10.1101/2024.09.21.614276; this version posted September 23, 2024. The copyright holder for this preprint (which was not certified by peer review) is the author/funder, who has granted bioRxiv a license to display the preprint in perpetuity. It is made available under a CC-BY 4.0 International license.

68 cortical neurons and astrocytes (18–22). These studies show that SARS-CoV-2 has both a neuroinvasive
69 and neurotropic potential, although the frequency of neuroinvasion is not well understood.

70

71 Neurovirulence of SARS-CoV-2 infection is its ability to cause lesions in the CNS leading to clinical
72 disease, independent of direct infection of CNS cells (3). Several mechanisms, such as microgliosis and
73 astrogliosis, are thought to contribute to the neurovirulence of SARS-CoV-2 infection. The activation
74 of microglia (microgliosis) and astrocytes (astrogliosis) is characterized by morphological changes of
75 these cell types as well as their influx into affected areas. In deceased COVID-19 patients, more
76 extensively ramified microglia were detected in the olfactory bulb, white matter and medulla
77 oblongata (11,23,24), as well as an increased influx of microglia into the olfactory bulb, meninges,
78 brainstem and cerebellum (7,11,25–27). Astrogliosis was observed in grey and white matter, in the
79 olfactory bulb, frontal cortex, medulla oblongata, cerebellum and basal ganglia of COVID-19 patients
80 (7,11,24). Transcriptomic analysis comparing post-mortem brain tissues of control and COVID-19
81 patients revealed a significant enrichment of astrocyte-associated genes in the amygdala potentially
82 indicating activation of astrocytes (6). Similar to humans, microglial activation in the olfactory bulb,
83 hippocampus, cortex and medulla oblongata was also observed in experimentally inoculated mice and
84 hamsters (17,23,24,28). Furthermore, enlargement of astrocytes was observed in the olfactory bulb
85 and hippocampus of hamsters (28), while another study failed to report an influx of astrocytes in the
86 olfactory bulb, cortex, medulla oblongata and hippocampus of SARS-CoV-2 inoculated hamsters (24).

87

88 Altogether, *in vivo* studies have shown that SARS-CoV-2 has a neuroinvasive and neurovirulent
89 potential in humans and animal models for moderate to severe respiratory disease, like mouse and
90 hamster. Whether SARS-CoV-2 infection can also induce neurovirulence during a subclinical or mild
91 infection is currently unknown, Therefore we investigated the neuroinvasive and neurovirulent
92 potential of SARS-CoV-2 in the ferret (*Mustela putorius furo*) that develop subclinical to mild

bioRxiv preprint doi: https://doi.org/10.1101/2024.09.21.614276; this version posted September 23, 2024. The copyright holder for this preprint (which was not certified by peer review) is the author/funder, who has granted bioRxiv a license to display the preprint in perpetuity. It is made available under a CC-BY 4.0 International license.

93 respiratory disease. Here, we characterized the neuroinvasive and neurovirulent potential of the
94 ancestral SARS-CoV-2 in intranasally inoculated ferrets, and investigated the presence of histological
95 lesions, viral RNA, and virus-infected cells, as well as numbers and surface areas of microglia and
96 astrocytes in the ferret brains. In this study, ferrets have been examined at the acute and post-acute
97 phase of SARS-CoV-2 infection. We determined acute phase up to 10 dpi, when the virus has not yet
98 been cleared, and the post-acute phase after 10 dpi, which can potentially provide insights into long-
99 COVID.

100

101

bioRxiv preprint doi: https://doi.org/10.1101/2024.09.21.614276; this version posted September 23, 2024. The copyright holder for this preprint (which was not certified by peer review) is the author/funder, who has granted bioRxiv a license to display the preprint in perpetuity. It is made available under a CC-BY 4.0 International license.

Materials and Methods

Animal experiments and tissues collection

Tissues were included in this study from intranasally inoculated SARS-CoV-2 ferrets from a previous study conducted in compliance with the Dutch legislation (29) for the protection of animals used for scientific purposes (2014, implementing EU Directive 2010/63) and other relevant regulations. All animal experiments were performed under BSL-3 conditions at Erasmus MC. In short, influenza A virus, SARS-CoV-2 and Aleutian Disease Virus seronegative male and female ferrets (Triple F Farms, PA, USA; between 1-2 years old) were intranasally inoculated with 10^5 $TCID_{50}$/ml SARS-CoV-2 D614G (isolate BetaCoV/Munich/BavPat1/2020). Only female ferrets that did not receive any treatment were included in this study. Four ferrets were sacrificed 7 days post inoculation (dpi), and three ferrets were sacrificed 21 dpi. Three age-matched and sex-matched non-inoculated ferrets were used as negative control for comparison of histological scoring.

The brain, trigeminal nerve, tip of the nose, nasal septum, and the nasal turbinates, which contained olfactory and respiratory mucosa were sampled for histopathological analysis (Fig 1A). Tissues were fixed in 10% formalin for two weeks. Transverse sections of the fixed brain were made at 0.5 cm intervals to evaluate spatial differences in histopathological changes and subsequently embedded in paraffin (Fig 1A).

Immunohistochemistry and histopathology

Three-µm-thick formalin-fixed paraffin-embedded (FFPE) tissue sections were deparaffinized, rehydrated and stained with haematoxylin (Klinipath) and eosin (QPath; H&E) to assess histopathological changes. For immunohistochemistry (IHC), consecutive tissue sections were deparaffinized, rehydrated and pre-treated for antigen retrieval. Pre-treatment of slides consisted of

bioRxiv preprint doi: https://doi.org/10.1101/2024.09.21.614276; this version posted September 23, 2024. The copyright holder for this preprint (which was not certified by peer review) is the author/funder, who has granted bioRxiv a license to display the preprint in perpetuity. It is made available under a CC-BY 4.0 International license.

boiling for 15 minutes in citric acid buffer (pH 6.0) for the detection of SARS-CoV-2 nucleoprotein (NP) and GFAP (glial fibrillary acidic protein; astrocytes); or boiling for 15 minutes in TRIS-EDTA buffer (pH 9.0) for the detection of IBA1 (ionized calcium binding adaptor molecule 1; microglia). After antigen retrieval, slides were incubated with 3% hydrogen peroxidase (Sigma-Aldrich) for 10 minutes to block endogenous peroxidases. After blocking, slides were washed with phosphate-buffered saline (PBS), and PBS/0.05% Tween 20 (Merck). Sections for SARS-CoV-2 IHC were additionally blocked with 10% goat serum (X0907, DAKO) for 30 minutes at room temperature (RT). Slides were incubated with a rabbit polyclonal antibody against SARS-CoV/SARS-CoV-2-nucleoprotein (40143-T62, Sino Biological, 1:1000), rabbit anti-IBA1 (019-19741, Wako Pure Chemical Corporation; 2.5 µg/ml) or mouse anti-GFAP (clone 4A11, BD556327, Biosciences, 20 µg/ml) in PBS/0,1% BSA (Aurion) for 1h at RT. For each staining on each tissue an isotype control was included as a negative control, either a rabbit IgG isotype control (AB-105-C, R&D, 1:200; 2.5 µg/ml), or mouse IgG2b isotype control (MAB0041, R&D, 5 µg/ml). Tissue sections from negative control ferrets were included as negative tissue controls for all stainings. A lung section from an experimentally inoculated hamster with SARS-CoV-2 was used as positive control for the NP SARS-CoV-2 IHC. After washing, sections were incubated with peroxidase labelled goat-anti-Rabbit IgG (P0448, DAKO, 1:100) or goat-anti-mouse IgG (PO447, Southern Biotech, 1:100) in PBS/0,1% BSA for 1 hour at RT. Peroxidase activity was revealed by incubating slides in 3-amino9-ethylcarbazole (AEC; Tokyo Chemical Industry) in N,N-dimethylformamide (DMF; Sigma-Aldrich) for 10 minutes, resulting in bright red precipitate, followed by counterstaining with haematoxylin (Sigma-Aldrich).

RNA isolation and qPCR

RNA was extracted from paraffin sections of all available tissues using the RNeasy FFPE kit (Qiagen) according to the manufacturer's protocol. In short, sections of 5 µM were collected in Eppendorf vials and deparaffinized using xylene. The sample was lysed with proteinase K digestion followed by heat

bioRxiv preprint doi: https://doi.org/10.1101/2024.09.21.614276; this version posted September 23, 2024. The copyright holder for this preprint (which was not certified by peer review) is the author/funder, who has granted bioRxiv a license to display the preprint in perpetuity. It is made available under a CC-BY 4.0 International license.

and DNAse treatment. Ethanol and RBC buffer from the kit was added to bind total RNA to the spin columns. Samples were washed and eluted twice in RNAse free water. qPCR was performed targeting E-gene of SARS-CoV-2 as previously reported (30). For the qPCR, the maximum RNA input was used, which corresponds to 100 ng input. The housekeeping gene hypoxanthine phosphoribosyltransferase 1 (HPRT) was included as control; its sequence can be found in (31). All reactions were run on a 7500 Real Time PCR Cycler (Applied Biosystems) in technical duplicates. A Ct-value < 45 was considered positive. Values are depicted ± SD. For the brain, all separate tissue sections were tested individually, but the average is depicted ± SD.

SARS-CoV-2 in situ hybridization

BaseScope™ RNA probes were designed by Bio-Techne Ltd (Abingdon, UK) for SARS-CoV-2 BA-V-CoV-Wuhan-Nucleocapsid-3zz-st (846661). In situ hybridization (ISH) was performed on FFPE consecutive sections using BaseScope™ Reagent Kit v2–RED (323900) as described by the manufacturer. SARS-CoV-2 nucleocapsid RNA molecules were visualized as red chromogenic dots.

Microscopy

H&E sections of all tissues were evaluated for histopathological changes with an Olympus BX51 light microscope by an certified veterinary pathologist. A 40× digital scan was made of H&E slides of the hindbrain (area surrounding the pons and cerebellum) for counting Alzheimer type II astrocytes using a Hamamatsu Nanozoomer 2.0 HT digital slide scanner with the accompanying software (NanoZoomer Digital Pathology and NDP.scan and NDP.view, Hamamatsu, Higashiku, Hamamatsu City, Japan). For microglial and astrocytic evaluation, a 10× air objective (Olympus) was used to select a region of interest with an Olympus BX51 microscope. The regions of interest for microglial and astrocytic evaluation in this study were determined as the glomerular layer and the granular cell layer of the olfactory bulb, the white matter tract (corpus callosum), grey matter (posterior parietal cortex) and

bioRxiv preprint doi: https://doi.org/10.1101/2024.09.21.614276; this version posted September 23, 2024. The copyright holder for this preprint (which was not certified by peer review) is the author/funder, who has granted bioRxiv a license to display the preprint in perpetuity. It is made available under a CC-BY 4.0 International license.

the hippocampus (CA1 region). We chose these areas, like the corpus callosum, to consistently sample in the same brain area, and therefore a ferret brain atlas was used to determine the correct area for imaging (32). The slides were blinded before the images of the selected regions of interest were taken. Images were taken at either a 200× magnification (20× air objective; Olympus) or 400× magnification (40× air objective; Olympus) with CellSense software.

Quantitative analysis of IBA1$^+$ cells, GFAP$^+$ cells and Alzheimer type II astrocytes

At least two sections per brain area were selected per ferret, and per section at least three images were taken of the region of interest in the brain. The number of IBA1$^+$ (microglia) and GFAP$^+$ (astrocytes) cells per high power field (400× magnification) was determined by manual counting by two observers blinded to the infection status. The averages ± SD of the IBA1$^+$ or GFAP$^+$ cells per ferret were plotted. As a measure for activation of astrocytes and microglia, the surface areas of IBA1$^+$ and GFAP$^+$ cells was determined using the pixel classifier function in QuPath 0.4.4 (33) with a Gaussian filter. The threshold values to determine the positive and negative surface areas can be found in Table 1. The averages ± SD of the IBA1$^+$ and GFAP$^+$ cells surface areas per ferret were plotted. Additionally, the surface area per IBA1$^+$ or GFAP$^+$ cell was plotted ± SD.

Alzheimer type II astrocytes were counted manually from a 40× digital scan of a H&E slide in Qupath 0.4.4 if the cell matched to the description referenced before (34,35). Alzheimer type II astrocytes are characterized by a large, pale nucleus, with a rim of chromatin and a small conspicuous nucleolus. The total brain area in the slide was calculated in µm^2 in Qupath 0.4.4 (33), and the number of Alzheimer type II astrocytes was normalized to number of cells per mm^2 brain area and plotted ± SD.

Table 1. The chosen threshold values used in QuPath to determine the IBA1$^+$ and GFAP$^+$ surface area

bioRxiv preprint doi: https://doi.org/10.1101/2024.09.21.614276; this version posted September 23, 2024. The copyright holder for this preprint (which was not certified by peer review) is the author/funder, who has granted bioRxiv a license to display the preprint in perpetuity. It is made available under a CC-BY 4.0 International license.

Region of interest	IBA1⁺ surface area	GFAP⁺ surface area
Glomerular layer (olfactory bulb)	0.12	N.P.
Granular cell layer (olfactory bulb)	0.12	N.P.
White matter (corpus callosum)	0.23	0.20
Grey matter (posterior parietal cortex)	0.18	0.21
Hippocampus (CA1 region)	0.17	0.17

N.P. = not performed, IBA1 = ionized calcium binding adaptor molecule 1, GFAP = glial fibrillary acidic protein.

Statistical analysis

Statistical differences between experimental groups were determined by using a one-way analysis of variance (ANOVA) with a Dunnett's *posthoc* test using GraphPad Prism version 10.1.2. P values of ≤ 0.05 were considered statistically significant. Figures were prepared with Adobe Photoshop 22.1.1 and Adobe Illustrator 25.1.0.

Results

Assessment of ferret respiratory tissues

To evaluate cell tropism in the respiratory tract of D614G SARS-CoV-2 intranasally inoculated ferrets were sacrificed at 7 or 21 days post inoculation (dpi) and samples of the tip of the nose, nasal septum, nasal turbinates containing olfactory and respiratory mucosa were analysed. As reported earlier, SARS-CoV-2 RNA was detected by qPCR in swabs of the throat and nose of these ferrets still at 7 dpi (29). Additionally, infectious virus was detected in throat swabs of these ferrets at 3 dpi (29). In our analyses on the FFPE tissues, at 7 dpi, viral RNA was detected in tissues of the nasal septum and nasal turbinates in all ferrets (Table 2). At 21 dpi, viral RNA was detected in the tip on the nose (1 out of 3 ferrets) and

bioRxiv preprint doi: https://doi.org/10.1101/2024.09.21.614276; this version posted September 23, 2024. The copyright holder for this preprint (which was not certified by peer review) is the author/funder, who has granted bioRxiv a license to display the preprint in perpetuity. It is made available under a CC-BY 4.0 International license.

nasal turbinates (2 out of 3 ferrets; Table 2). ISH verified the presence of the SARS-CoV-2 viral RNA in all qPCR-positive respiratory tissue sections (Table 2). Next, to determine the location and cellular tropism of SARS-CoV-2 in the ferret respiratory tract, IHC for SARS-CoV-2 NP was performed. Virus antigen could not be detected in the tip of the nose or nasal septum from ferrets sacrificed at 7 and 21 dpi. Virus antigen was detected at 7 dpi in both respiratory and olfactory mucosa of the nasal turbinates, but was more pronounced in the ciliated respiratory mucosa cells (Fig 1B). The presence of virus antigen was associated with inflammation, characterized by slight to mild infiltration of neutrophils within the mucosal lamina propria and within the epithelial lining in the respiratory mucosa and in a lesser extent in the olfactory mucosa. Additionally, necrotic sloughed epithelial debris admixed with few neutrophils was present within nasal passages along the inflamed mucosae in one ferret (Fig 1B). Virus antigen or histopathological changes of significance were not detected in the respiratory tissues of ferrets sacrificed at 21 dpi, although sporadic numbers of neutrophils were still present within the lamina propria and within the epithelial lining of the respiratory mucosa of two ferrets (Fig 1C).

Table 2. Ct-values of viral RNA detected in various tissues of SARS-CoV-2 inoculated ferrets.

			Ferret						
	Days post inoculation	**Target**	**#1**	**#2**	**#3**	**#4**	**#5**	**#6**	**#7**
Nasal turbinates	7	S2	32.2	28.3	27.0	32.8			
		HPRT	37.9	37.2	34.5	34.1			
	21	S2					37.3	N.D.	32.8
		HPRT					39.0	34.9	34.8
Tip of the nose	7	S2	N.D.	N.D.	N.D.	N.D.			
		HPRT	36.1	35.5	37.2	34.7			
	21	S2					N.D.	39.1	N.A.
		HPRT					36.8	36.4	N.A.
Nasal Septum	7	S2	36.6	35.9	34.1	33.0			
		HPRT	35.9	38.2	37.2	34.2			
	21	S2					N.D.	N.D.	N.D.
		HPRT					39.5	35.8	38.9
Trigeminal	7	S2	N.D.	N.D.	N.D.	N.A.			

bioRxiv preprint doi: https://doi.org/10.1101/2024.09.21.614276; this version posted September 23, 2024. The copyright holder for this preprint (which was not certified by peer review) is the author/funder, who has granted bioRxiv a license to display the preprint in perpetuity. It is made available under a CC-BY 4.0 International license.

nerve		HPRT	37.2	37.7	37.1	N.A.			
	21	S2					N.D.	N.A.	N.D.
		HPRT					38.7	N.A.	42.0
Brain (pooled)	7	S2	41.5	39.0	38.6	38.5			
		HPRT	37.5	36.6	35.4	35.3			
	21	S2					N.D.	N.D.	N.D.
		HPRT					37.1	35.4	36.1

S2 = SARS-CoV-2; HPRT = hypoxanthine phosphoribosyltransferase 1 (housekeeping gene); N.D. = not detected, Ct-value ≥ 45; N.A. = not available; Nasal turbinates contain both respiratory and olfactory mucosa; Brain (pooled) is pooled data from all positive qPCR brain tissue sections.

Assessment of the neuroinvasive potential of SARS-CoV-2 in ferrets

Next, we investigated the neuroinvasive potential of D614G SARS-CoV-2 in ferrets, by testing for viral RNA by qPCR and virus antigen expression by IHC. If viral RNA was detected, we verified this by ISH. Viral RNA was detected by qPCR in inoculated ferrets sacrificed at 7 dpi in various parts of the brain (pooled results of various qPCR positive brain tissues sections in Table 2). However, virus antigen was not detected by IHC in any ferrets and ISH did not confirm the presence of viral RNA in qPCR-positive brain tissues.

Assessment of histopathological changes in the brain

All brain areas were screened for histopathological abnormalities. We did not detect infiltration of any inflammatory cells, and no gliosis or necrosis in the brain tissues of any ferret. Alzheimer type II astrocytes were detected in the area of the pons and the cerebellum (example in Fig 2A). We observed significantly more Alzheimer type II astrocytes in SARS-CoV-2 inoculated ferrets sacrificed at 7 and 21 dpi compared to control (Fig 2B). The number of Alzheimer type II astrocytes in ferrets sacrificed at 21 dpi were significantly lower compared to ferrets sacrificed at 7 dpi (Fig 2B).

bioRxiv preprint doi: https://doi.org/10.1101/2024.09.21.614276; this version posted September 23, 2024. The copyright holder for this preprint (which was not certified by peer review) is the author/funder, who has granted bioRxiv a license to display the preprint in perpetuity. It is made available under a CC-BY 4.0 International license.

Assessment of neurovirulence in the olfactory bulb

Expression of IBA1 (microglia) and GFAP (astrocytes) was determined in the brain of D614G inoculated ferrets by IHC to characterize neurovirulence. IBA1 expression in the glomerular layer of olfactory bulbs appeared to be modestly increased by qualitative visual examination in ferrets sacrificed at 7 dpi and 21 dpi compared to the control ferrets (Fig 3A). Quantitative analysis revealed no significant differences in the number of $IBA1^+$ cells between control and infected ferrets in both the glomerular and granular cell layers of the olfactory bulb (Fig 3B, C). However, there was a significant increase in the $IBA1^+$ surface area per high power field (HPF) in the glomerular layer of the olfactory bulb in ferrets sacrificed at 7 and 21 dpi compared to control ferrets (Fig 3B). Analysis of the surface area normalized per $IBA1^+$ cell did not differ significantly between infected and control ferrets in the glomerular layer and granular cell layer of the olfactory bulb (Fig 3B, C). The GFAP expression did not appear to be different between control and infected ferrets (Fig 3D). Quantification of the number and surface area of $GFAP^+$ cells was not feasible in the olfactory bulb, because GFAP expression was to widespread and therefore it was not possible to distinguish single cells, which is required for quantification.

Assessment of neurovirulence in, white and grey matter of cerebral cortex and the hippocampus

IBA1 and GFAP IHC was performed to investigate the activation status of microglia and astrocytes, respectively, in the white and grey matter of the cerebral cortex (corpus callosum and posterior parietal cortex, respectively) and the hippocampus (CA1 region). Again, quantitative analyses were performed per brain area: counting the number of $IBA1^+$ or $GFAP^+$ cells and measuring the $IBA1^+$ or $GFAP^+$ surface area per HPF (Fig 4). The main trends were as follows. In the white matter, no statistically significant differences in the number of $IBA1^+$ cells, surface area or surface area per $IBA1^+$ cell were observed (Fig 4A), while significantly less $GFAP^+$ surface area was detected (Fig 4B). In the grey matter,

bioRxiv preprint doi: https://doi.org/10.1101/2024.09.21.614276; this version posted September 23, 2024. The copyright holder for this preprint (which was not certified by peer review) is the author/funder, who has granted bioRxiv a license to display the preprint in perpetuity. It is made available under a CC-BY 4.0 International license.

no statistically significant differences were observed in the number of IBA1$^+$ and GFAP$^+$ and their surface area (Fig 4C, D). In the hippocampus, a statistically significant increase in IBA1$^+$ surface area was detected (Fig 4E) in inoculated ferrets sacrificed at 7 and 21 dpi compared to control ferrets, while a decrease in GFAP$^+$ surface was seen in ferrets sacrificed at 7 dpi compared to control ferrets (Fig 4F).

Discussion

This study demonstrates that SARS-CoV-2 has limited neuroinvasive potential via the olfactory route in this ferret model, although neuroinvasion via the hematogenous route or neuroinvasion at earlier timepoints cannot be excluded. We observed SARS-CoV-2 replication in the respiratory and olfactory mucosa confirming other studies (4,5,14,16,17,29). The ability of SARS-CoV-2 to replicate in the olfactory mucosa in experimentally inoculated ferrets that develop mild respiratory disease, increases the likelihood that virus can spread to the brain via the olfactory nerve as observed in influenza A virus-infected ferrets (36) or in SARS-CoV-2 infected hamsters (17).

Subtle changes were observed in the brains of SARS-CoV-2 inoculated ferrets, despite the lack of evidence for neuroinvasion. These changes included microgliosis and a decrease in astrocytic activation, as well as, an increase in Alzheimer type 2 astrocytes and were present in the acute and post-acute phase. Microglia and astrocytes can be reactive upon direct infection or direct stimuli in their environment such as the presence of viruses or other pathogens in surrounding cells (17,37–42). Another way for increased activation is through indirect stimuli like proinflammatory cytokines caused by a systemic response to for example viral infection (40,41), or a combination of all above. Increased microglial activation upon SARS-CoV-2 infection was observed in patients and experimentally inoculated mice and hamsters, which can be models for severe respiratory disease (7,11,17,23–28). Microglia play a crucial role in maintaining brain homeostasis in health and disease, synapse formation, neuronal proliferation, and brain development. Dysregulation of these processes can impact learning

bioRxiv preprint doi: https://doi.org/10.1101/2024.09.21.614276; this version posted September 23, 2024. The copyright holder for this preprint (which was not certified by peer review) is the author/funder, who has granted bioRxiv a license to display the preprint in perpetuity. It is made available under a CC-BY 4.0 International license.

and memory, and deficits have been associated with increased and prolonged microglial activation after infection with SARS-CoV-2, but also with other viruses like influenza A viruses (43–45).

The role of astrocytic activation and Alzheimer type II astrocytes triggered by SARS-CoV-2 infection has been less studied. One study reported an increase in astrocytic activation (28), while another study reported no differences in a hamster model (24). The functional consequences of decreased astrocyte activation are currently unknown, but altered astrocyte physiology can modulate both astrocytic and neuronal glutamate transporter trafficking and activity (46). Thus, a reduction of the reactive astrocyte marker GFAP, meaning that the astrocytes are in a less reactive state, can play a role in dysregulation of glutamate signaling. Altered glutamate signaling is implicated in neuropsychiatric disorders and neurodegenerative diseases, which are both associated with SARS-CoV-2 infection (26,40,43,47,48). Alzheimer type II astrocytes, which we detected in the hindbrain, have recently been detected in the brain of a COVID-19 infected patient. This patient was diagnosed with viral meningoencephalitis with symptoms like altered consciousness and seizures (25). Alzheimer type II astrocytes may be an indicator of hepatic encephalopathy (35,49) but have not been studied extensively. The implications of the presence of Alzheimer type II astrocytes after SARS-CoV-2 infection are currently unknown and need to be studied more.

Together, these data suggest that the ferret serves as a model for self-limiting to mild respiratory disease with limited neuroinvasive potential. Even though the lack of evidence for neuroinvasion, the infection still induced neurovirulence evident by microglial activation, astrocytic deactivation and Alzheimer type II astrocytes. So far, the neuropathogenesis has mainly been studied in animal models for severe disease, while this study highlights the value of this ferret model to study the effects on the brain after mild respiratory disease following intranasal SARS-CoV-2 infection in the acute and post-acute phase.

Acknowledgements

bioRxiv preprint doi: https://doi.org/10.1101/2024.09.21.614276; this version posted September 23, 2024. The copyright holder for this preprint (which was not certified by peer review) is the author/funder, who has granted bioRxiv a license to display the preprint in perpetuity. It is made available under a CC-BY 4.0 International license.

This work was funded in part by a fellowship from the Netherlands Organization for Scientific Research (VIDI contract 91718308). Ferret experiments were previously published and supported by funding from the National Institutes of Health (AI146980, AI121349, NS091263, AI114736, HHSN272201400008C).

Author Contributions

Conceptualization: Feline F. W. Benavides, Debby van Riel, Lisa Bauer

Data Curation: Feline F. W. Benavides, Lonneke Leijten

Formal analysis: Feline F. W. Benavides, Edwin J. B. Veldhuis Kroeze, Lonneke Leijten

Funding Acquisition: Rory de Vries, Debby van Riel

Investigation: Feline F. W. Benavides, Lonneke Leijten, Edwin J. B. Veldhuis Kroeze, Peter van Run

Methodology: Katharina S. Schmitz, Rory D. de Vries, Feline F. W. Benavides, Lonneke Leijten

Project Administration: Feline F. W. Benavides, Katharina S. Schmitz, Rory D. de Vries, Debby van Riel, Lisa Bauer

Resources: Katharina S. Schmitz, Rory D. de Vries

Software: Feline F. W. Benavides

Supervision: Debby van Riel, Lisa Bauer, Thijs Kuiken

Validation: Edwin J.B. Veldhuis Kroeze, Feline F. W. Benavides, Lonneke Leijten

Visualization: Feline F. W. Benavides

Writing – Original Draft Preparation: Feline F. W. Benavides, Lisa Bauer, Thijs Kuiken, Debby van Riel

Writing – Review & Editing: all authors

bioRxiv preprint doi: https://doi.org/10.1101/2024.09.21.614276; this version posted September 23, 2024. The copyright holder for this preprint (which was not certified by peer review) is the author/funder, who has granted bioRxiv a license to display the preprint in perpetuity. It is made available under a CC-BY 4.0 International license.

References

1. Graham EL, Clark JR, Orban ZS, Lim PH, Szymanski AL, Taylor C, e.a. Persistent neurologic symptoms and cognitive dysfunction in non-hospitalized Covid-19 'long haulers'. Ann Clin Transl Neurol. May 2021;8(5):1073-85.

2. Fernández-de-Las-Peñas C, Cancela-Cilleruelo I, Rodríguez-Jiménez J, Arias-Navalón JA, Martín-Guerrero JD, Pellicer-Valero OJ, e.a. Trajectory of post-COVID brain fog, memory loss, and concentration loss in previously hospitalized COVID-19 survivors: the LONG-COVID-EXP multicenter study. Front Hum Neurosci. 2023;17:1259660.

3. Bauer L, Laksono BM, de Vrij FMS, Kushner SA, Harschnitz O, van Riel D. The neuroinvasiveness, neurotropism, and neurovirulence of SARS-CoV-2. Trends Neurosci. May 2022;45(5):358-68.

4. de Melo GD, Lazarini F, Levallois S, Hautefort C, Michel V, Larrous F, e.a. COVID-19-related anosmia is associated with viral persistence and inflammation in human olfactory epithelium and brain infection in hamsters. Science Translational Medicine. 2021;13(596).

5. Meinhardt J, Radke J, Dittmayer C, Franz J, Thomas C, Mothes R, e.a. Olfactory transmucosal SARS-CoV-2 invasion as a port of central nervous system entry in individuals with COVID-19. Nat Neurosci. February 2021;24(2):168-75.

6. Serrano GE, Walker JE, Tremblay C, Piras IS, Huentelman MJ, Belden CM, e.a. SARS-CoV-2 Brain Regional Detection, Histopathology, Gene Expression, and Immunomodulatory Changes in Decedents with COVID-19. J Neuropathol Exp Neurol. Augustus 2022;81(9):666-95.

7. Al-Dalahmah O, Thakur KT, Nordvig AS, Prust ML, Roth W, Lignelli A, e.a. Neuronophagia and microglial nodules in a SARS-CoV-2 patient with cerebellar hemorrhage. Acta Neuropathol Commun. Augustus 2020;8(1):147.

8. Khan M, Yoo SJ, Clijsters M, Backaert W, Vanstapel A, Speleman K, e.a. Visualizing in deceased COVID-19 patients how SARS-CoV-2 attacks the respiratory and olfactory mucosae but spares the olfactory bulb. Cell. November 2021;184(24):5932-5949.e15.

9. Hansen T, Titze U, Kulamadayil-Heidenreich NSA, Glombitza S, Tebbe JJ, Röcken C, e.a. First case of postmortem study in a patient vaccinated against SARS-CoV-2. Int J Infect Dis. June 2021;107:172-5.

10. Cama VF, Marín-Prida J, Acosta-Rivero N, Acosta EF, Díaz LO, Casadesús AV, e.a. The microglial NLRP3 inflammasome is involved in human SARS-CoV-2 cerebral pathogenicity: A report of three post-mortem cases. J Neuroimmunol. December 2021;361:577728.

bioRxiv preprint doi: https://doi.org/10.1101/2024.09.21.614276; this version posted September 23, 2024. The copyright holder for this preprint (which was not certified by peer review) is the author/funder, who has granted bioRxiv a license to display the preprint in perpetuity. It is made available under a CC-BY 4.0 International license.

11. Matschke J, Lütgehetmann M, Hagel C, Sperhake JP, Schröder AS, Edler C, e.a. Neuropathology of patients with COVID-19 in Germany: a post-mortem case series. Lancet Neurol. November 2020;19(11):919-29.

12. Remmelink M, De Mendonça R, D'Haene N, De Clercq S, Verocq C, Lebrun L, e.a. Unspecific post-mortem findings despite multiorgan viral spread in COVID-19 patients. Crit Care. Augustus 2020;24(1):495.

13. Stein SR, Ramelli SC, Grazioli A, Chung JY, Singh M, Yinda CK, e.a. SARS-CoV-2 infection and persistence in the human body and brain at autopsy. Nature. December 2022;612(7941):758-63.

14. Monchatre-Leroy E, Lesellier S, Wasniewski M, Picard-Meyer E, Richomme C, Boué F, e.a. Hamster and ferret experimental infection with intranasal low dose of a single strain of SARS-CoV-2. J Gen Virol. March 2021;102(3):001567.

15. Shimizu S, Nakayama M, Nguyen CT, Ishigaki H, Kitagawa Y, Yasui F, e.a. SARS-CoV-2 induces inflammation and intracranial infection through the olfactory epithelium-olfactory bulb pathway in non-human primates. J Neuroimmunol. February 2024;387:578288.

16. van de Ven K, van Dijken H, Wijsman L, Gomersbach A, Schouten T, Kool J, e.a. Pathology and Immunity After SARS-CoV-2 Infection in Male Ferrets Is Affected by Age and Inoculation Route. Front Immunol. 2021;12:750229.

17. Bauer L, Rissmann M, Benavides FFW, Leijten L, van Run P, Begeman L, e.a. In vitro and in vivo differences in neurovirulence between D614G, Delta And Omicron BA.1 SARS-CoV-2 variants. Acta Neuropathol Commun. September 2022;10(1):124.

18. Song E, Zhang C, Israelow B, Lu-Culligan A, Prado AV, Skriabine S, e.a. Neuroinvasion of SARS-CoV-2 in human and mouse brain. J Exp Med. March 2021;218(3):e20202135.

19. Bauer L, Lendemeijer B, Leijten L, Embregts CWE, Rockx B, Kushner SA, e.a. Replication Kinetics, Cell Tropism, and Associated Immune Responses in SARS-CoV-2- and H5N1 Virus-Infected Human Induced Pluripotent Stem Cell-Derived Neural Models. mSphere. June 2021;6(3):e0027021.

20. Yang L, Han Y, Nilsson-Payant BE, Gupta V, Wang P, Duan X, e.a. A Human Pluripotent Stem Cell-based Platform to Study SARS-CoV-2 Tropism and Model Virus Infection in Human Cells and Organoids. Cell Stem Cell. July 2020;27(1):125-136.e7.

21. Andrews MG, Mukhtar T, Eze UC, Simoneau CR, Ross J, Parikshak N, e.a. Tropism of SARS-CoV-2 for human cortical astrocytes. Proc Natl Acad Sci U S A. July 2022;119(30):e2122236119.

22. Kong W, Montano M, Corley MJ, Helmy E, Kobayashi H, Kinisu M, e.a. Neuropilin-1 Mediates SARS-CoV-2 Infection of Astrocytes in Brain Organoids, Inducing Inflammation Leading to Dysfunction and Death of Neurons. mBio. December 2022;13(6):e0230822.

bioRxiv preprint doi: https://doi.org/10.1101/2024.09.21.614276; this version posted September 23, 2024. The copyright holder for this preprint (which was not certified by peer review) is the author/funder, who has granted bioRxiv a license to display the preprint in perpetuity. It is made available under a CC-BY 4.0 International license.

23. Fernández-Castañeda A, Lu P, Geraghty AC, Song E, Lee MH, Wood J, e.a. Mild respiratory COVID can cause multi-lineage neural cell and myelin dysregulation. Cell. July 2022;185(14):2452-2468.e16.

24. Soung AL, Vanderheiden A, Nordvig AS, Sissoko CA, Canoll P, Mariani MB, e.a. COVID-19 induces CNS cytokine expression and loss of hippocampal neurogenesis. Brain. December 2022;145(12):4193-201.

25. Duarte-Neto AN, Caldini EG, Gomes-Gouvêa MS, Kanamura CT, de Almeida Monteiro RA, Ferranti JF, e.a. An autopsy study of the spectrum of severe COVID-19 in children: From SARS to different phenotypes of MIS-C. EClinicalMedicine. May 2021;35:100850.

26. Eschbacher KL, Larsen RA, Moyer AM, Majumdar R, Reichard RR. Neuropathological findings in COVID-19: an autopsy cohort. J Neuropathol Exp Neurol. December 2022;82(1):21-8.

27. Stoyanov GS, Petkova L, Dzhenkov DL, Sapundzhiev NR, Todorov I. Gross and Histopathology of COVID-19 With First Histology Report of Olfactory Bulb Changes. Cureus. December 2020;12(12):e11912.

28. Kishimoto-Urata M, Urata S, Kagoya R, Imamura F, Nagayama S, Reyna RA, e.a. Prolonged and extended impacts of SARS-CoV-2 on the olfactory neurocircuit. Sci Rep. April 2022;12(1):5728.

29. de Vries RD, Schmitz KS, Bovier FT, Predella C, Khao J, Noack D, e.a. Intranasal fusion inhibitory lipopeptide prevents direct-contact SARS-CoV-2 transmission in ferrets. Science. March 2021;371(6536):1379-82.

30. Corman VM, Landt O, Kaiser M, Molenkamp R, Meijer A, Chu DK, e.a. Detection of 2019 novel coronavirus (2019-nCoV) by real-time RT-PCR. Eurosurveillance. January 2020;25(3):2000045.

31. Carolan LA, Butler J, Rockman S, Guarnaccia T, Hurt AC, Reading P, e.a. TaqMan real time RT-PCR assays for detecting ferret innate and adaptive immune responses. J Virol Methods. September 2014;205:38-52.

32. Radtke-Schuller S. Cyto- and myeloarchitectural brain atlas of the ferret (Mustela putorius) in MRI aided stereotaxic coordinates. 1st edition 2018. Cham: Springer International Publishing; 2018. 310 p.

33. Bankhead P, Loughrey MB, Fernández JA, Dombrowski Y, McArt DG, Dunne PD, e.a. QuPath: Open source software for digital pathology image analysis. Sci Rep. December 2017;7(1):16878.

34. Norenberg MD. Astrocyte responses to CNS injury. J Neuropathol Exp Neurol. May 1994;53(3):213-20.

35. Norenberg MD. The role of astrocytes in hepatic encephalopathy. Neurochem Pathol. 1987;6(1-2):13-33.

bioRxiv preprint doi: https://doi.org/10.1101/2024.09.21.614276; this version posted September 23, 2024. The copyright holder for this preprint (which was not certified by peer review) is the author/funder, who has granted bioRxiv a license to display the preprint in perpetuity. It is made available under a CC-BY 4.0 International license.

36. van den Brand JMA van den, Stittelaar KJ, Amerongen G van, Reperant L, Waal L de, Osterhaus ADME, e.a. Comparison of Temporal and Spatial Dynamics of Seasonal H3N2, Pandemic H1N1 and Highly Pathogenic Avian Influenza H5N1 Virus Infections in Ferrets. PLOS ONE. Augustus 2012;7(8):e42343.

37. Meinhardt J, Streit S, Dittmayer C, Manitius RV, Radbruch H, Heppner FL. The neurobiology of SARS-CoV-2 infection. Nat Rev Neurosci. January 2024;25(1):30-42.

38. Jurgens HA, Amancherla K, Johnson RW. Influenza infection induces neuroinflammation, alters hippocampal neuron morphology, and impairs cognition in adult mice. J Neurosci. March 2012;32(12):3958-68.

39. Colonna M, Butovsky O. Microglia Function in the Central Nervous System During Health and Neurodegeneration. Annu Rev Immunol. April 2017;35:441-68.

40. Chagas L da S, Serfaty CA. The Influence of Microglia on Neuroplasticity and Long-Term Cognitive Sequelae in Long COVID: Impacts on Brain Development and Beyond. Int J Mol Sci. March 2024;25(7):3819.

41. Ramesh G, MacLean AG, Philipp MT. Cytokines and chemokines at the crossroads of neuroinflammation, neurodegeneration, and neuropathic pain. Mediators Inflamm. 2013;2013:480739.

42. Potokar M, Zorec R, Jorgačevski J. Astrocytes Are a Key Target for Neurotropic Viral Infection. Cells. September 2023;12(18):2307.

43. Braga J, Lepra M, Kish SJ, Rusjan PM, Nasser Z, Verhoeff N, e.a. Neuroinflammation After COVID-19 With Persistent Depressive and Cognitive Symptoms. JAMA Psychiatry. Augustus 2023;80(8):787-95.

44. Hosseini S, Wilk E, Michaelsen-Preusse K, Gerhauser I, Baumgärtner W, Geffers R, e.a. Long-Term Neuroinflammation Induced by Influenza A Virus Infection and the Impact on Hippocampal Neuron Morphology and Function. J Neurosci. 21 2018;38(12):3060-80.

45. Hosseini S, Michaelsen-Preusse K, Schughart K, Korte M. Long-Term Consequence of Non-neurotropic H3N2 Influenza A Virus Infection for the Progression of Alzheimer's Disease Symptoms. Front Cell Neurosci. April 2021;15:643650.

46. Hughes EG, Maguire JL, McMinn MT, Scholz RE, Sutherland ML. Loss of glial fibrillary acidic protein results in decreased glutamate transport and inhibition of PKA-induced EAAT2 cell surface trafficking. Brain Res Mol Brain Res. May 2004;124(2):114-23.

47. Jaywant A, Vanderlind WM, Alexopoulos GS, Fridman CB, Perlis RH, Gunning FM. Frequency and profile of objective cognitive deficits in hospitalized patients recovering from COVID-19. Neuropsychopharmacology. December 2021;46(13):2235-40.

48. Mazza MG, De Lorenzo R, Conte C, Poletti S, Vai B, Bollettini I, e.a. Anxiety and depression in COVID-19 survivors: Role of inflammatory and clinical predictors. Brain Behav Immun. October 2020;89:594-600.

bioRxiv preprint doi: https://doi.org/10.1101/2024.09.21.614276; this version posted September 23, 2024. The copyright holder for this preprint (which was not certified by peer review) is the author/funder, who has granted bioRxiv a license to display the preprint in perpetuity. It is made available under a CC-BY 4.0 International license.

498 49. Albrecht J, Jones EA. Hepatic encephalopathy: molecular mechanisms underlying the
499 clinical syndrome. J Neurol Sci. November 1999;170(2):138-46.

500

bioRxiv preprint doi: https://doi.org/10.1101/2024.09.21.614276; this version posted September 23, 2024. The copyright holder for this preprint (which was not certified by peer review) is the author/funder, who has granted bioRxiv a license to display the preprint in perpetuity. It is made available under a CC-BY 4.0 International license.

Figure legends:

Fig 1. Histology and presence of SARS-CoV-2 antigen expression in the respiratory and olfactory mucosae of SARS-CoV-2 inoculated ferrets. Intranasally inoculated ferrets (D614G; 10^5 $TCID_{50}$) were sacrificed at day 7 or day 21 post inoculation. Tissues sampled are depicted in (A) left panel: 1 = tip of the nose; 2 = nasal cavity containing respiratory and olfactory mucosa; 3 = olfactory bulb; and 4 = the brain within the cranial cavity; 5 = trigeminal nerve. As shown in the right panel, transverse sections of the fixed brain were made at 0.5 cm intervals to evaluate spatial differences in histopathological changes. Hematoxylin and eosin (H&E) staining and immunohistochemistry (IHC) staining for SARS-CoV-2 nucleoprotein of the respiratory mucosa (B) and olfactory mucosa (C) of SARS-CoV-2 inoculated ferrets. Individual columnar ciliated epithelial cells in the respiratory mucosa collected at 7 dpi express cytoplasmic SARS-CoV-2 antigen (B, lower row) colocalized with infiltration of neutrophils, and intraluminal presence of cellular debris also containing few neutrophils (B, upper row).

Fig 2. Detection of Alzheimer type II astrocytes in the area of the pons and cerebellum of inoculated ferrets. (A) A 40× digital scan was used for counting Alzheimer type II astrocytes (example with yellow arrows), which were characterized by having a large, pale nucleus with a rim of marginated chromatin and small conspicuous nucleolus. (B) The number of Alzheimer type II astrocytes were counted in a brain slice and normalized to number of cells per mm^2. Statistical significance was calculated with a one-way analysis of variance (ANOVA) with a Dunnett's *posthoc* test. Averaged values of three or four individual ferrets per infection group were compared to values of three control ferrets. Data is shown as mean ± SD. Asterisks indicate statistical significance (*P<0.05, **P<0.01, ***P<0.001).

Fig 3. Activation status of microglia and astrocytes in the olfactory bulb of SARS-CoV-2 inoculated ferrets. (A) Detection of microglial ($IBA1^+$) cells in the glomerular and granular cell layer of the olfactory bulbs of SARS-CoV-2 inoculated ferrets. The number of $IBA1^+$ cells and $IBA1^+$ surface area in the glomerular layer (B) and granular cell layer (C) of the olfactory bulb. Statistical significance was

bioRxiv preprint doi: https://doi.org/10.1101/2024.09.21.614276; this version posted September 23, 2024. The copyright holder for this preprint (which was not certified by peer review) is the author/funder, who has granted bioRxiv a license to display the preprint in perpetuity. It is made available under a CC-BY 4.0 International license.

526 calculated with a one-way analysis of variance (ANOVA) with a Dunnett's *posthoc* test. Averaged values
527 of three or four individual ferrets per infection group were compared to values of three control ferrets.
528 Data shown as mean ± SD. Asterisks indicate statistical significance (*P<0.05). (D) Detection of
529 astrocytes ($GFAP^+$) cells in the glomerular and granular cell layer of olfactory bulb of inoculated ferrets.
530 Abbreviations: HPF = high power field, IBA1 = ionized calcium binding adaptor molecule 1, GFAP = glial
531 fibrillary acidic protein.

532

533 **Fig 4. The activation status of microglia and astrocytes in the white matter, grey matter and**
534 **hippocampus of SARS-CoV-2 infected ferrets.** (A) Number of $IBA1^+$ cells, the $IBA1^+$ surface area and
535 the surface area per cell in the white matter. (B) Number of $GFAP^+$ cells, the $GFAP^+$ surface area and
536 the surface area per cell in the white matter. (C) Number of $IBA1^+$ cells, the $IBA1^+$ surface area and the
537 surface area per cell in the grey matter. (D) Number of $GFAP^+$ cells, the $GFAP^+$ surface area and the
538 surface area per cell in the grey matter. (E) Number of $IBA1^+$ cells, the $IBA1^+$ surface area and the
539 surface area per cell in the hippocampus (CA1 region). (F) Number of $GFAP^+$ cells, the $GFAP^+$ surface
540 area and the surface area per cell in the hippocampus (CA1 region). Statistical significance was
541 calculated with a one-way analysis of variance (ANOVA) with a Dunnett's *posthoc* test. Averaged values
542 of three or four individual ferrets per infection group were compared to values of three control ferrets.
543 Data shown as mean ± SD. Asterisks indicate statistical significance (*P<0.05, **P<0.01). Abbreviations:
544 HPF = high power field, IBA1 = ionized calcium binding adaptor molecule 1, GFAP = glial fibrillary acidic
545 protein.

546

bioRxiv preprint doi: https://doi.org/10.1101/2024.09.21.614276; this version posted September 23, 2024. The copyright holder for this preprint (which was not certified by peer review) is the author/funder, who has granted bioRxiv a license to display the preprint in perpetuity. It is made available under a CC-BY 4.0 International license.

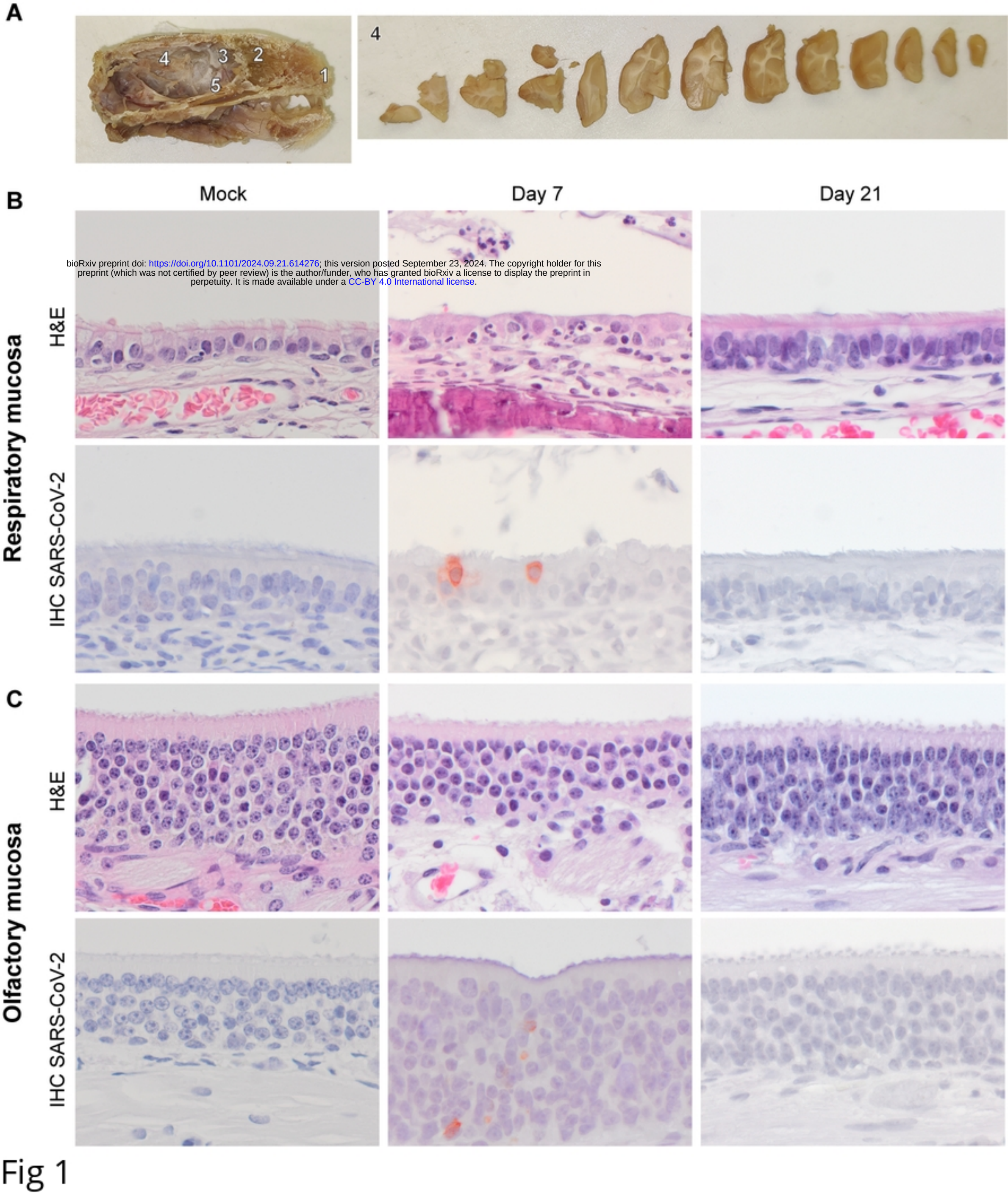


Fig 1

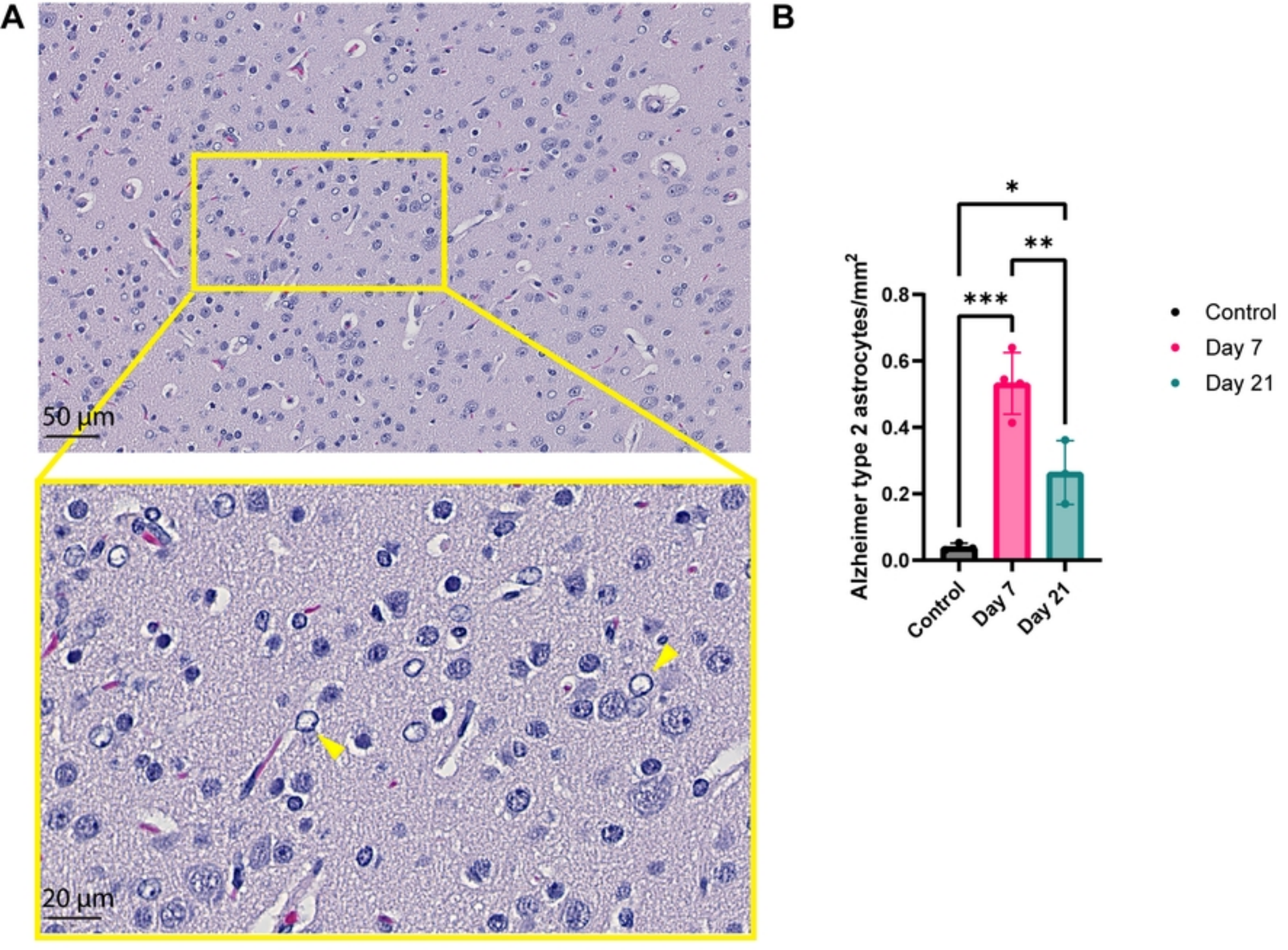

A
50 µm
20 µm
B
Alzheimer type 2 astrocytes/mm²
0.0
0.2
0.4
0.6
0.8
*
**
***
Control
Day 7
Day 21
Control
Day 7
Day 21

Fig 2

bioRxiv preprint doi: https://doi.org/10.1101/2024.09.21.614276; this version posted September 23, 2024. The copyright holder for this preprint (which was not certified by peer review) is the author/funder, who has granted bioRxiv a license to display the preprint in perpetuity. It is made available under a CC-BY 4.0 International license.

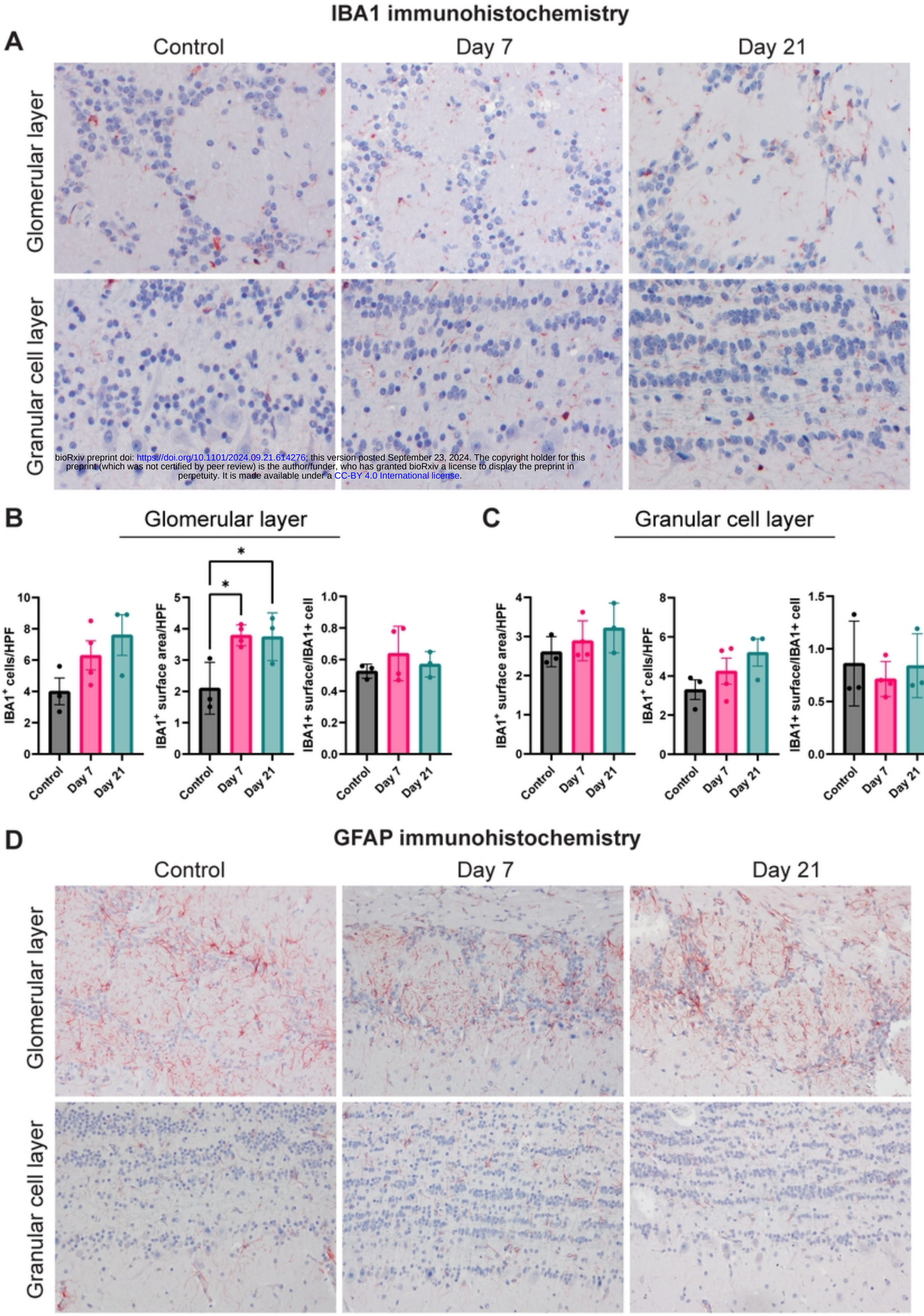


Fig 3

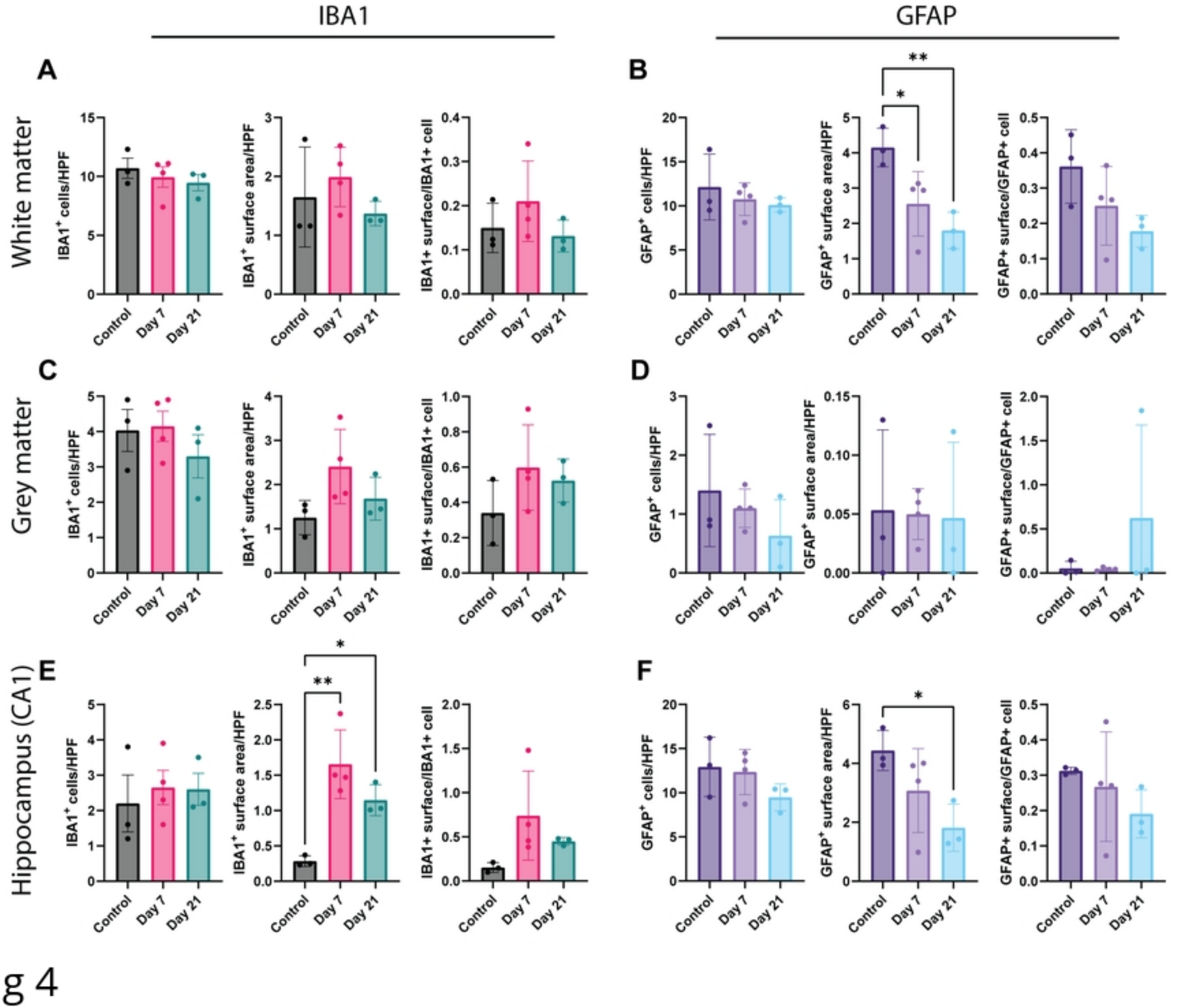

IBA1
GFAP
A
B
C
D
E
F
White matter
Grey matter
Hippocampus (CA1)
IBA1+ cells/HPF
IBA1+ surface area/HPF
IBA1+ surface/IBA1+ cell
GFAP+ cells/HPF
GFAP+ surface area/HPF
GFAP+ surface/GFAP+ cell
Control
Day 7
Day 21
*
**

Fig 4